Supplementary Material

Imaging the proton concentration and mapping the spatial distribution of the electric field of catalytic micropumps

A. Afshar-Farniya, M.J. Esplandiu, D. Reguera, A. Bachtold

I- Tracing particles and zeta potential

We use three different tracing particles: 2 μm diameter polystyrene spheres (Kisker Biotech GmbH & Co), 2 μm diameter polystyrene spheres functionalized with amidine groups (Invitrogen), and 1.5 μm diameter silica spheres (Kisker Biotech GmbH & Co). The zeta potentials are determined in a 1% H_2O_2 solution with a Malvern ZetaSizer Nano ZS Instrument.

II- Cleaning treatment of micropumps

Micropumps are fabricated using standard electron-beam lithography techniques. They are subjected to 30 minutes of piranha cleaning and one minute of oxygen plasma cleaning (0.8 mbar, 500 Watt) to remove residual PMMA/organic contamination. This treatment is critical to observe the motion of the fluid and the particles. The treatment also modifies the electrochemical behavior of gold and platinum (see section III). XPS measurements are performed to follow-up the surface treatment. The relative atomic concentrations of oxygen for both treated and non-treated gold and platinum surfaces are calculated by integrating the peak area of the O1s signal and applying its relative sensitivity factor (RSF) and normalizing over all the elements detected. We find that, in the case of Au, the atomic concentration of oxygen increases by a factor of 9 (from 3% to 27%) after the cleaning treatment. In the case of Pt, the oxygen increases by a factor of 4 (from 9.4% to 39.9%) after the cleaning treatment. We also characterize the changes in the spectra of the Au and Pt signals. Figure S1 shows the XPS spectra for Au4f and Pt4f for the sample treated with plasma (a and c) compared to their analogs without treatment (b and d). The untreated samples show the typical doublet due to the metallic bond. However, in the treated samples, additional shoulders at higher energies can be observed. These shoulders are shifted by about 1.7 eV for Au and 2.8eV for Pt with respect to the metallic peaks. Such shoulders correspond to oxidized states of Au and Pt. These results show that the cleaning treatment changes the surface chemistry of the metals.

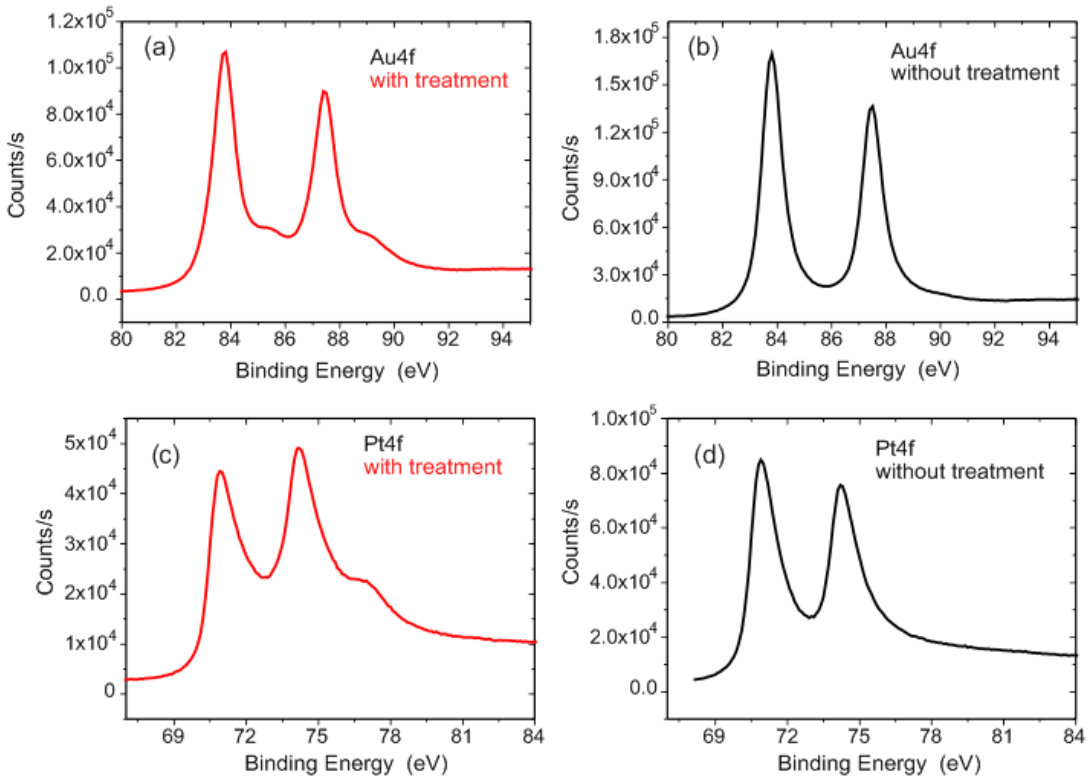

Figure S1. XPS spectra for Au and Pt treated samples (a and c) as compared to the untreated ones (b and d).

III- Tafel measurements

Tafel measurements consist in recording the electrochemical current as a function of the potential difference between a liquid and a metal electrode. We use it to determine the mixed potentials of platinum and gold, that is, the potential at which there is no net redox reaction and the current is zero. Figures S2 (a) and (b) show Tafel curves obtained for gold and platinum electrodes. These electrodes are fabricated by evaporating either gold or platinum on a wafer and subjected to the cleaning treatment (section II). Different electrolytes are used: 1 wt% hydrogen peroxide with supporting electrolyte (phosphate buffer solution with pH= 7.4) [Fig. S2 (a)] and 1 wt% hydrogen peroxide without supporting electrolyte [Fig. S2 (b)]. The scan rate is set to 1 mV/s. The mixed potential of platinum is higher than the one of gold (0.22V and 0.16 V, respectively, for the solution with supporting electrolyte and 0.39 V and 0.25 V, respectively, for the solution without supporting electrolyte). As a result, platinum acts as the cathode and gold as the anode for hydrogen peroxide decomposition. These results are independent of the way the metals are evaporated: similar results are obtained using Joule and electron-beam evaporation. However, when the metal electrodes are not subjected to the cleaning treatment (section II), the mixed potential of gold is similar to that of platinum.

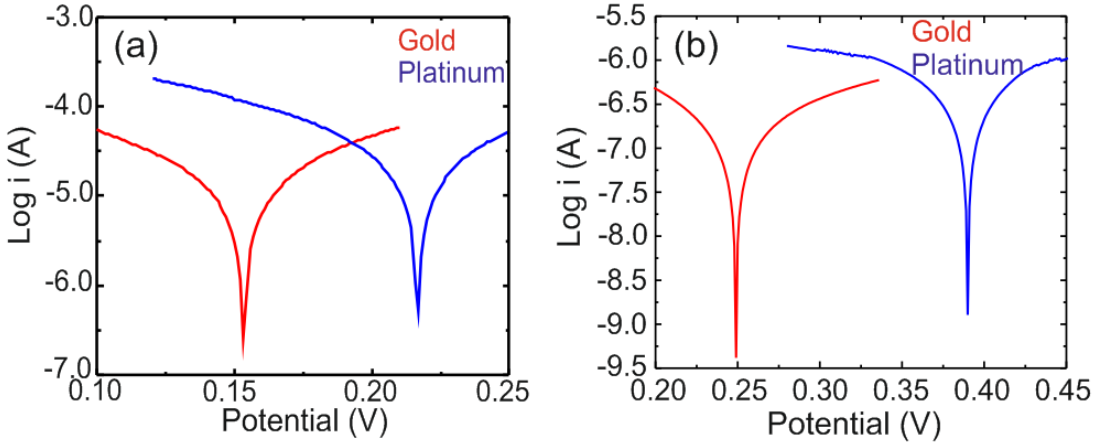

Figure S2. Tafel plots for gold and platinum electrodes in 1% hydrogen peroxide and phosphate buffer solution (a) and without the supporting electrolyte (b).

IV- Motility studies

A 8 mm diameter and 0.12 mm thick gasket-like spacer (Invitrogen) is placed on top of the wafer patterned with micropumps. A 1 wt% hydrogen peroxide solution containing particles is added to the vacant space created by the gasket. The wafer is immediately capped with a thin glass cover. The motion of particles is recorded at 5 frames per second rate and analyzed with the Diatrack software to determine their velocity.

V- Motion of particles

Positively charged particles. Figure 1b-e in the paper shows a p^+ particle that moves towards the cathode disk in the plane parallel to the disk surface. Figure S3 shows an example where the motion is not parallel to the disk surface. The particle is first in a plane out of focus, at more than 10 µm away from the surface; it then ends on the disk surface. The particle has a velocity component in the z axis that is downwards, in the opposite direction of the upwards flow of the liquid. The downwards motion of the p^+ particle is attributed to the electric field. Importantly, it also suggests that the electric field remains significant in the bulk of the liquid away from the electric double layer.

Quasi-neutral particles. Quasi-neutral polystyrene particles move towards the disk. Once they arrive to the disk edge, they either change the direction of the motion and move in the direction normal to the disk (Fig. S4b) or get adsorbed on the surface (Fig. S4a).

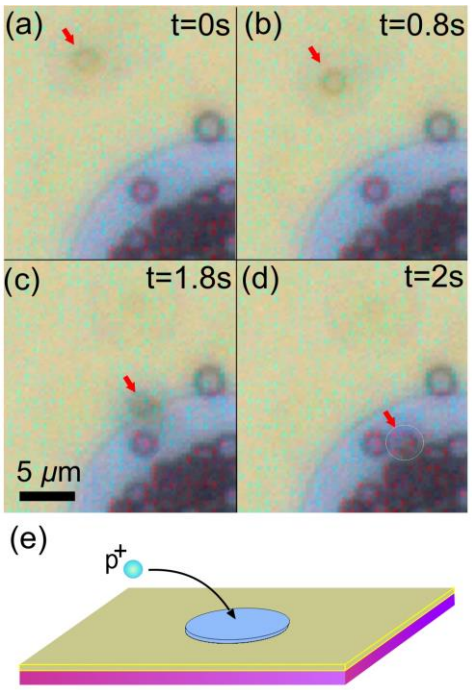

Fig. S3 Motion of a positively charged particle. The particle has a velocity component in the z axis that points downwards.

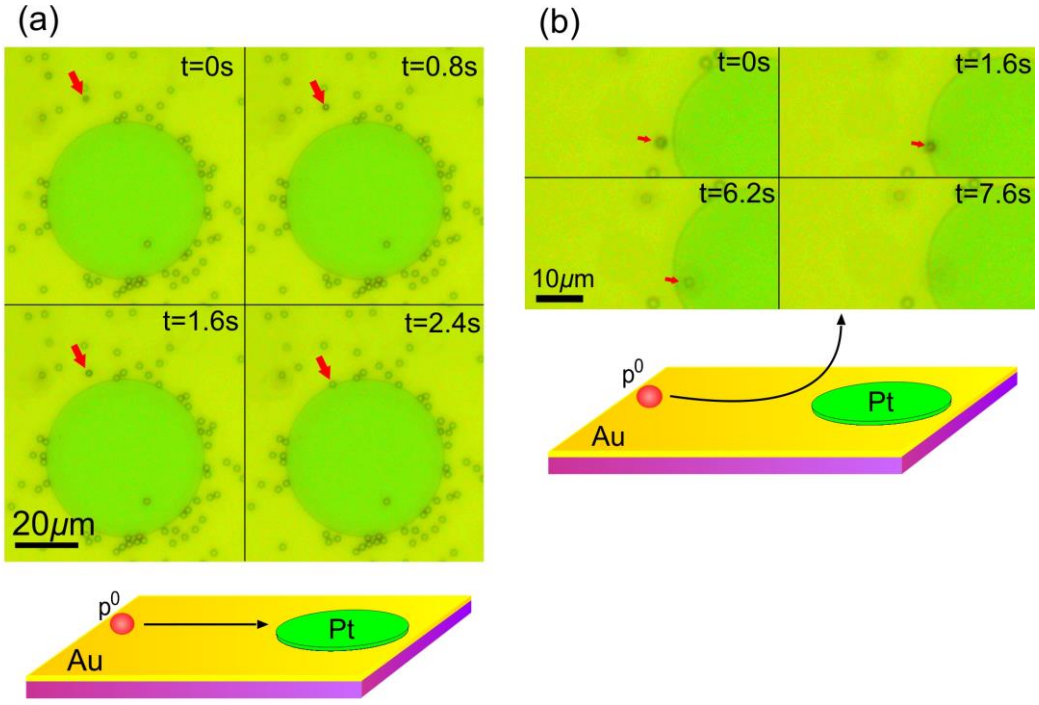

Fig. S4. Motion of quasi-neutral particles. (a) The particle gets adsorbed at the disk edge. (b) The particle moves in the direction normal to the disk; the particle gets out of focus and eventually disappears. The color of the gold and the platinum is different from that in Fig. S3, since we used another filter.

Negatively charged particles. Figure S5 shows that p^- particles do not approach the disk. A band without particles is formed around the disk due to the repulsion induced by the electric field.

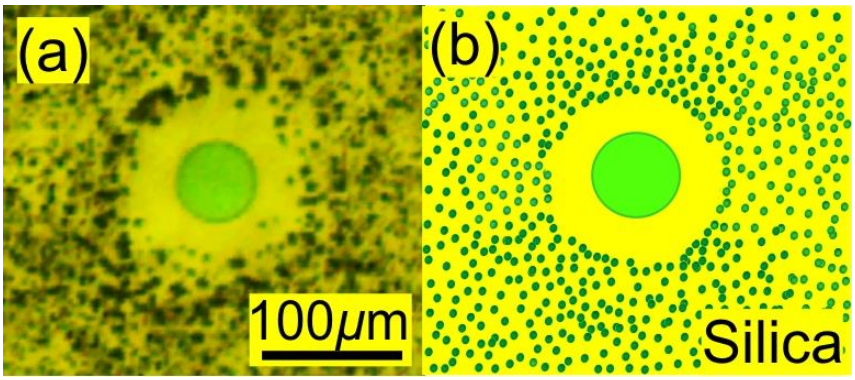

Fig. S5. Response of negatively charged particles.

VI- Fluorescent pH indicator and confocal fluorescence microscopy

The fluorescence measurements are performed with a Leica TCS SP5 confocal microscope equipped with an AOBS system (Acousto-optical Beam splitter), which provides high quality imaging. We used pyranine as pH indicator with a pKa of about 7 (Fig. S6). This fluorophore exhibits dual excitation, which allows ratiometric measurements which is an ideal methodology to eliminate possible artifacts, such as lack of dye concentration uniformity, photobleaching, etc [1]. The molecule is excited at 405 and 458 nm and the emission is collected from 480 to 580 nm. At 405 nm the fluorescence intensity decreases as the pH increases, whereas the fluorescence signal increases as the pH increases when the dye is excited at 458 nm. Figure S6a shows the calibration curves at both excitation wavelengths as a function of different pH solutions in absence of H_2O_2 and with a dye concentration of 5μM. We also checked that the fluorescent intensity of the dye is not altered in presence of 1% H_2O_2. The figure additionally shows the color scale in order to get an idea of the general trends at both wavelengths. In ratiometric measurements, the pH depends on the ratio between the fluorescence signals at the two wavelengths. Figure S6b shows the ratio as a function of pH.

To evaluate the pH, we use the standard calibration equation in terms of the ratio of fluorescence signals,

$$pH = pK_a - log\left[\frac{R-R_B}{R_A-R} \times \frac{F_{B(\lambda 2)}}{F_{A(\lambda 2)}}\right] \quad \text{(S1)}$$

where pKa is 7, R is the ratio of the fluorescence signals at the two wavelengths, R_B is the ratio of the fluorescence signals in the basic extreme (pH=9), R_A is the ratio of the fluorescence signals in the acidic extreme (pH=4), F_B and F_A are the fluorescence signals at the acidic and

basic extreme for one of the wavelengths (e.g. λ= 458 nm). As mentioned in the manuscript, we get proton concentration images by applying this equation pixel by pixel. Figures S7 a and b show fluorescence intensity images taken at λ=405 nm and λ=458 nm respectively.

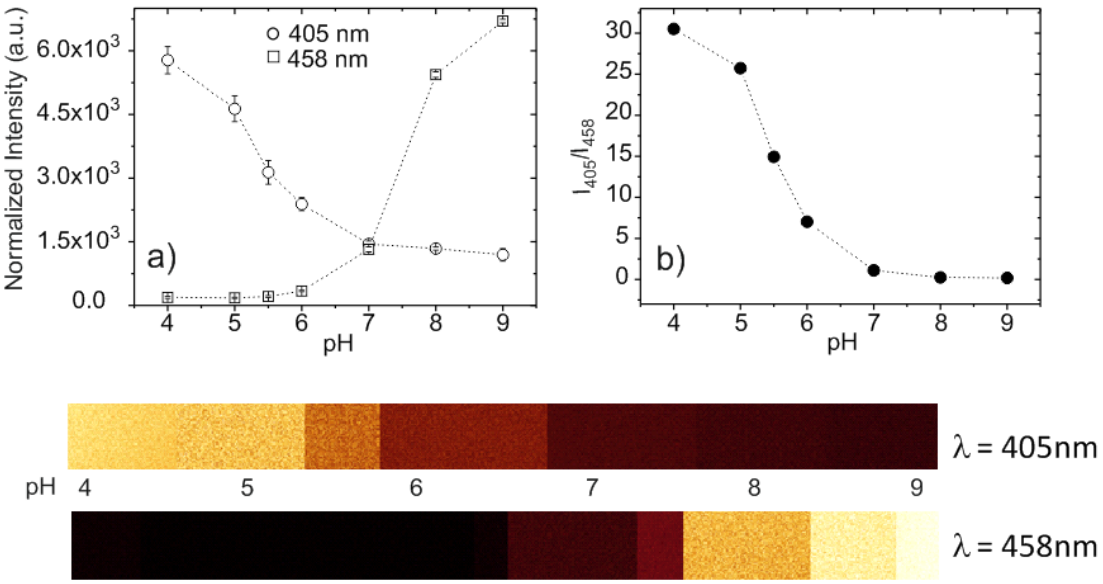

Figure S6. a) Fluorescence intensity as a function of pH. (b) Fluorescence signal ratio as a function of pH. Bottom part= fluorescence intensity palette as a function of pH for both wavelengths.

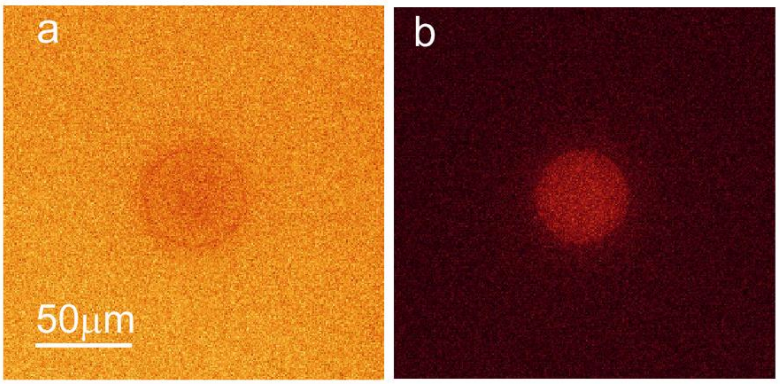

Figure S7. Fluorescence images of the device in presence of 1% H_2O_2 at λ=405 nm (a) and λ=458 nm (b).

We also check the response of the micropump in absence of hydrogen peroxide. Figure S8 shows the fluorescence response at the two excitation wavelengths in absence of H_2O_2 and at a pH solution of 7. It can be observed that the fluorescence is nearly uniform over the surface.

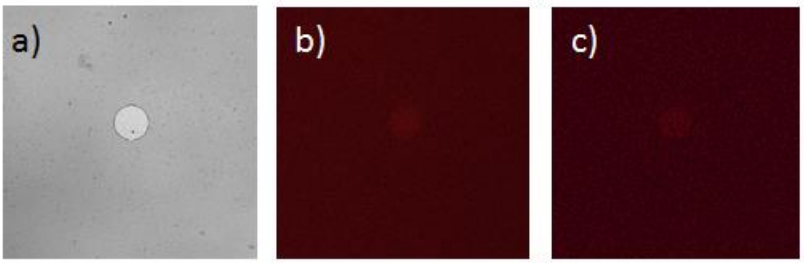

Figure S8. a) Reflectance image of the micropump together with its confocal fluorescence images without H_2O_2 at 405 nm (b) and 458 nm (c) . The fluorescence intensity remains quite homogenous over the surface.

VII- Finite element simulations

The finite element simulations are performed with Comsol Multiphysics by solving the following coupled governing equations at steady state conditions.

Poisson equation: $$-\varepsilon\nabla^2\varphi = \rho_e \quad \text{(S2)}$$

where $\varepsilon = \varepsilon_r\varepsilon_0$ is the permittivity of the liquid, φ is the electrostatic potential, and ρ_e is the total charge density.

Navier Stokes equation: $$\eta\nabla^2 \mathrm{v} = \nabla p + \rho_e\nabla\varphi \quad \text{(S3)}$$

$$\nabla\cdot \mathrm{v} = 0 \quad \text{(S4)}$$

where v is the fluid velocity, p is the pressure, η is the fluid viscosity, and the fluid is considered as incompressible.

Nernst-Planck equation: $$\mathrm{v}\cdot\nabla \mathrm{C_i} = \nabla\cdot(\mathrm{D_i}\nabla \mathrm{C_i} + \mathrm{z_i F}\mu_\mathrm{i}\nabla\varphi) \quad \text{(S5)}$$

where *C* is the molar concentration, *D* is the diffusion coefficient, *z* is the valence, *F* is the Faraday constant, μ is the mobility and the subscript *i* denotes the species. The mobility is defined through the Nernst–Einstein equation as $D_i = \mu_i RT$. In our simulations, four different charged species are considered: protons, hydroxide ions, and a 1:1 salt. In the case of the salt a typical diffusion coefficient of $1.0\cdot 10^{-9} m^2 s^{-1}$ is considered for both species.

The layout of the modeled system with axial symmetry is depicted below (Fig. S9). The typical parameters used for the simulations are summarized in Table I.

We use the following boundary conditions. For the electrostatic potential:

$$\varphi(z = 60\mu m) = 0$$

$$\varphi(z = 0) = \varphi_{subs}$$

We consider the same zeta potential for Au and Pt. We use the value of -0.033V, which is extracted from our measurements. For the fluid velocity, stick boundary conditions are imposed on the substrate and slip conditions are imposed elsewhere. The concentrations of the different species are set to the bulk values in Table 1 at the upper boundary $z = 60\mu m$.

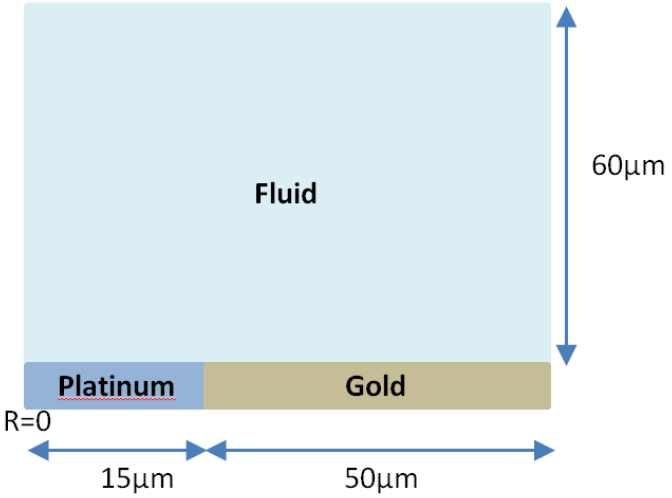

Figure S9. Layout with the typical dimensions used in the simulations.

Table 1. Parameters used in the simulations.

Description	**Values**
Proton's diffusion coefficient	$9.3\ 10^{-9}[m^2s^{-1}]$
OH's diffusion coefficient	$5.3\ 10^{-9}[m^2s^{-1}]$
Proton concentration in the bulk	pH=6.25
Zeta potential of Pt	-0.033V
Zeta potential of Au	-0.033 V
Rate constant k_{Pt}	$0.01\ [m^7s^{-1}\ mol^{-2}]$
Rate constant k_{Au}	$4.1\ 10^{-10}\ [m\ s^{-1}]$
H_2O_2 concentration	0.3M (1%)
Radius of the Pt disk	15 µm
Radius of gold ring	50 µm
Concentration of additional monovalent ions in the solution	1.6 µM

Description	Values
Diffusion coefficient of the additional ionic species	$1.0\ 10^{-9}[m^2s^{-1}]$

The following expressions (Ref. 2) are used to describe the current density of protons at the Au and Pt surfaces:

$$j_{Au} = k_{Au}\, C_{H2O2} \qquad \text{(S6)}$$

$$j_{Pt} = -k_{Pt}\, C_{H2O2}\, C_{H+}{}^{2} \qquad \text{(S7)}$$

C_i denotes the concentration of specie *i*. The values of the rate constants k_{Au} and k_{Pt} and the concentration of ion impurities are used as fitting parameters to reproduce the experimental results.

We incorporate in our simulations the presence of ion impurities in order to have a more realistic description of the experiments. Indeed, it is not possible to get completely ion free solutions, especially in the presence of microfabricated surfaces and colloidal dispersions. Figure S10 shows the calculated electric field as a function of the position for different concentrations of ion impurities.

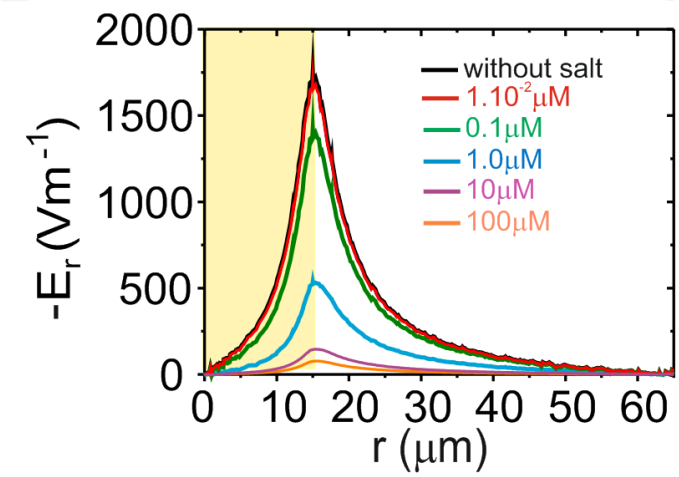

Figure S10. Influence of the concentration of ion impurities on the electric field

[1] J. Han J, K. Burgess, Chem Rev., **110**, 2709 (2010).

[2] J.L. Moran and J.D. Posner, J. Fluid Mech. **680**, 31 (2011).